UTILITY OF 4D RECONSTRUCTION FOR LOW-DOSE CARDIAC GATED SPECT

Mingwu Jin[1], Xiaofeng Niu[2], Wenyuan Qi[2], Yongyi Yang[2], Miles N. Wernick[2], and Michael A. King[3]

[1]Dept. of Physics, University of Texas at Arlington, Arlington, TX 76019
[2]Dept. of Electrical and Computer Engineering, Illinois Institute of Technology, Chicago, IL 60616
[3]Dept. of Radiology, University of Massachusetts Medical School, Worcester, MA 01655

ABSTRACT

By modeling major degrading factors in SPECT imaging along with motion-compensated temporal denoising, 4D reconstruction is demonstrated to significantly improve the quality of reconstructed images in cardiac gated SPECT (GSPECT) at the standard dose level. The utility of 4D reconstruction for radiation dose reduction in GSPECT has not been studied despite increased concern in population based risk due to its ionizing radiation. In this work, we investigate the potential of 4D reconstruction on reducing the imaging dose using Monte Carlo simulation of GSPECT imaging of a realistic human phantom at different dose levels. We use a number of metrics to quantify the quality of reconstructed images. The results demonstrate that 4D reconstruction can achieve better or comparable reconstruction at half dose compared to conventional clinical reconstruction at standard dose.

Index Terms— cardiac gated SPECT (GSPECT), 4D reconstruction, ionizing radiation, dose level.

1. INTRODUCTION

Currently 5 to 7 million SPECT myocardial perfusion imaging (MPI) studies are performed per year in the United States alone [1] and over 90% of them are ECG gated studies (GSPECT) [2]. Its high frequency use coupled with relatively high radiation dose leads to an estimated contribution of 20% of the annual collective radiation dose to the US population received from diagnostic procedures [3]. During a decade of follow-up in survivors of acute myocardial infarction, it was found that age and gender adjusted cancer risk increased by 3% for every 10 mSv of radiation used for MPI [4]. Therefore, there is an urgent need to lower the radiation dose used in SPECT MPI in order to reduce this population based cancer risk.

There were some preliminary results which demonstrated the feasibility of using advanced three-dimensional (3D) reconstruction, which incorporated noise suppression and resolution recovery, for dose reduction in SPECT MPI [5,6], while more efforts were focused on shortening the imaging time. A recent numerical observer study also suggested that there is some room to reduce acquisition time or injected activity without degrading performance on myocardial perfusion defect detection using 3D reconstruction [7].

The quality of SPECT images is limited by a number of factors, including Poisson noise, distance-dependent point spread function (PSF), attenuation, and scatter. The noise problem is especially serious in GSPECT, where the counts are further divided among different (8 or 16) gated intervals of the cardiac cycle. In order to achieve clinically satisfactory image quality, the tracer dose of GSPECT is typically three-fold of that in non-gated SPECT. 4D reconstruction methods that exploit the temporal correlation among the gated frames have been developed to improve image quality in GSPECT, aiming to achieve better perfusion defect detectability and functional assessment [8-14]. In [13], attenuation and scatter compensation as well as resolution recovery were integrated with motion-compensated temporal smoothing in 4D reconstruction. All these 4D studies were conducted with current standard dose. The utility of 4D reconstruction methods for the dose reduction has not been investigated. Lowering the radiation dose while maintaining (or improving) image quality can significantly improve the quality of patient care. As an added benefit, the demand on the radioisotope, such as ^{99m}Tc, can be substantially decreased at the same time.

In this work, we investigate the utility of 4D reconstruction [13] to lower the injected dose of GSPECT. We use Monte Carlo simulation [15] to simulate GSPECT acquisition of both standard and half dose with the 4D NURBS-based cardiac-torso (NCAT) phantom [16] and ^{99m}Tc-Sestamibi as the imaging agent. Images reconstructed by different reconstruction methods are used to assess the quantitative reconstruction accuracy as well as perfusion defect detection performance.

2. METHODS

2.1. 4D reconstruction

In GSPECT the cardiac cycle is divided into K intervals. We model the imaging process as

$$E[g_k]=Hf_k+r_k,\ k=1,2,\ldots,K, \quad (1)$$

in which g_k, f_k and r_k are vectors representing the projection data, original image, and expected scatter component, respectively, of the kth gate interval, $E[\bullet]$ is the expectation

This work was supported by the NIH under grant HL65425.

operator, and H is a matrix describing the imaging system ("system matrix").

The goal is to estimate the images f_k from the data g_k, k=1,…,K. The conventional clinical approach has been to reconstruct each gate frame separately using FBP or OSEM. In 4D reconstruction [13], we seek a simultaneous solution of all the frames f_k from Eq.(1), aiming to take advantage of both the spatial and temporal correlations among the gate frames. Both the distance-dependent PSF and the attenuation effect are modeled in the system matrix H based on the distance information from the point of interest to the detector face, the collimator geometry, and the attenuation map acquired through the transmission images. The scatter component is estimated by the triple-energy window method [13].

Let **F** denote collectively all gate image frames f_k, and similarly, **G** denote as all projection data. Then **F** is obtained by maximum *a posteriori* (MAP) estimation as

$$\hat{\mathbf{F}} = \arg\max_{\mathbf{F}} [\log p(\mathbf{G};\mathbf{F}) + \log p(\mathbf{F})], \qquad (2)$$

where p(**G**;**F**) is the likelihood function of **G** parameterized by **F**, which follows a Poisson distribution, and p(**F**) is a prior distribution of **F** that comprises of both spatial and temporal regularizations. In the prior term p(**F**) the degree of spatial and temporal smoothing is controlled by two parameters: spatial parameter β_s and temporal parameter β_t. More details of the 4D algorithm can be found in [13].

2.2. Phantom simulation data

In our experiments, the 4D NCAT 2.0 phantom [16] was used to generate the source and attenuation distribution. A female phantom (of which one transverse slice is shown in Fig. 1a) was generated with the following body size: 35.2 cm (long-axis) x 26.7 cm (short-axis) x 41.7 cm (height), and rib size: 24 cm x 18.2 cm x 29.8 cm. The simulated breast dimensions were 18.2 cm x 7.0 cm x 14.0 cm. The female phantom was used to introduce more significant breast and diaphragmatic attenuation.

The SIMIND Monte Carlo package [15] was used to simulate gated SPECT imaging with ^{99m}Tc-labeled Sestamibi as the imaging agent and with the Picker Prism3000 with low-energy high-resolution (LEHR) collimator as the imaging system. The projection matrix was 64 by 64 with a pixel size 0.634 cm. For a circular camera rotation of 28.5 cm radius, 64 projection sets were collected for each gated frame of total 16 gates. Two energy windows were used: the photopeak window was 20% (28 keV) centered at 140 keV, and a 3.5 keV window abutted to the lower side of the photopeak window for scatter correction. The scattered counts in the photopeak window were about 34% of the total counts. For a ^{99m}Tc-labeled Sestamibi study, Poisson noise was introduced at levels of 8 million (8M) total acquired counts as in a standard dose acquisition and 4 million (4M) as in a half-dose acquisition.

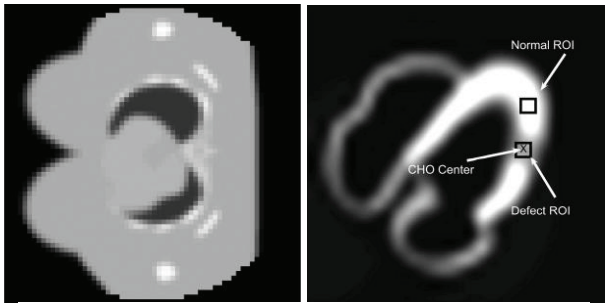


Fig.1 a) a transverse slice of the NCAT phantom (Left); b) defect location and ROIs for performance assessment (Right).

Two datasets (30 noise realizations in each) for each dose level were generated, one with a defect and the other without. A transmural perfusion defect with 50% intensity reduction was introduced in the anterior-lateral region of the LV (Fig. 1b).

2.3. Reconstruction methods

The following methods are used for comparison in our experiments.

(1) Clinical spatiotemporal method (ST121) [13]: the different gated frames are first reconstructed by FBP, then processed spatially with a Butterworth lowpass filter, and further processed along the gate dimension with a temporal filter with impulse response 1/4, 2/4, 1/4.

(2) 3D MAP reconstruction (3D): the different gated frames are reconstructed independently by MAP estimation, in which spatial prior is used to enforce spatial smoothing. This amounts to setting the temporal prior to zero in Eq.(2). For optimal results, the spatial parameter was varied as β_s=[0, 0.5, 2, 5, 7]×10^{-4} .

(3) 4D reconstruction: both the spatial and temporal priors are used in Eq.(2) and the gated frames are reconstructed simultaneously. The temporal parameter is chosen as β_t=5×10^{-4} (optimized as [13]), while the spatial parameter is varied in the same way as in 3D.

The distance-dependent PSF, attenuation, and scatter are included in methods (2) and (3) and the modified BSREM algorithm is used for reconstruction [13]. The method ST121 is used to reconstruct the data collected at the standard dose level ("ST121 8M"), which is used as a standard of the clinical practice. For comparison, all the above three methods are applied to data acquired at the half-dose level (denoted as "ST121 4M", "3D 4M", and "4D 4M"). As reference for quantitative analyses, the gated volumetric images are reconstructed using the OSEM algorithm from simulated noiseless projection of the phantom data without attenuation and scatter (by turning off attenuation and scatter in SIMIND), representing an ideal case achievable without degradations of attenuation, scatter, and noise (referred to as "Ideal" hereafter).

2.4. Evaluation metrics

To evaluate the quality of the reconstructed images, we compute a number of quantitative metrics, including: (1) overall error level of the myocardium measured by signal-to-noise ratio (SNR), (2) regional bias-variance analysis of the LV wall, (3) uniformity of the LV wall, (4) time activity curve (TAC) analysis of the LV wall, and (5) detectability of perfusion defects using channelized Hotelling observer (CHO) [17]. These metrics are used to quantify several different aspects of the reconstructed myocardium. The details of these metrics can be found in [13,14]. These metrics were computed from reconstruction with 30 noise realizations in the experiments.

3. RESUTLS AND DISCUSSIONS

We show in Fig. 2 the SNR results of the reconstructed myocardium with different reconstruction methods. Each curve was obtained by varying the spatial parameter. As expected, ST121 4M had lower SNR than ST121 8M due to the increased noise (lower counts). However, both 3D 4M and 4D 4M outperformed ST121 8M, thanks to the combination of denoising and correction for degradation factors in the reconstruction. 4D 4M achieved the best SNR (i.e. least error level).

We conducted bias-variance analyses on two ROIs on the LV wall (Fig. 1b). We show in Fig. 3 the bias-standard deviation plot of the normal ROI obtained with the different reconstruction methods. In this plot, each curve was obtained by varying the spatial parameter β_s. In each curve, the left-end point corresponds to β_s=0 (i.e., no spatial smoothing); thus, each curve shows a decreasing trend in variance but also an increasing trend in bias as the spatial parameter β_s is increased. There is only a small increase in variance but a notable increase in bias for ST121 4M compared to ST121 8M. Both 3D 4M and 4D 4M achieved significantly reduced bias compared to ST121 8M; 4D 4M also greatly decreased the variance in the reconstruction. Similar results were also obtained for the defect ROI but omitted here due to the space limitation.

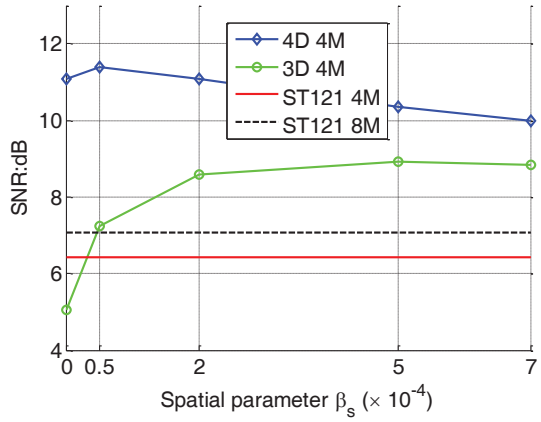


Fig. 2 Signal-to-noise ratio (SNR) of the myocardium reconstructed by different methods.

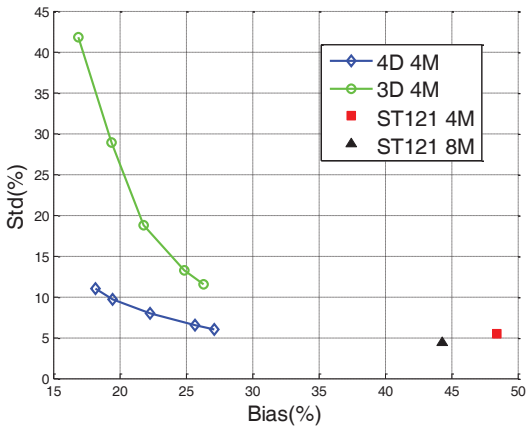


Fig. 3 Bias-standard deviation plot for the normal ROI reconstructed by different methods.

In Fig. 4 we show the defect detectability CHO results for the different methods, where the area under the receiver characteristic (ROC) curve (A_z) is plotted. A higher A_z value corresponds to the better detection performance. The best detection performance was obtained by 4D 4M, followed by ST121 8M. These results demonstrate that 4D reconstruction can lead to better defect detection even with the significantly reduced imaging dose (50%) compared to the clinical standard method (ST121 8M).

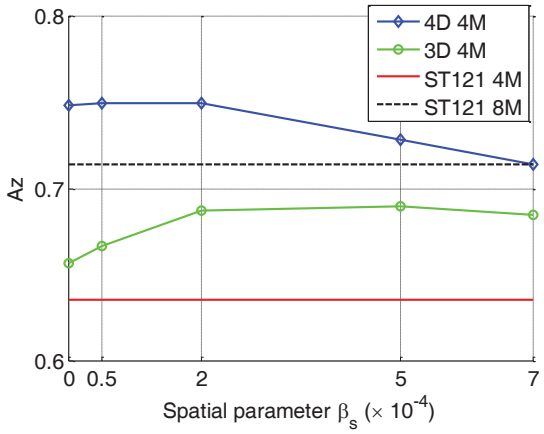


Fig.4 CHO detection Az results from different methods.

In Table 1 we show the uniformity results of the LV wall (a smaller value means higher uniformity). For 3D 4M and 4D 4M the spatial parameter β_s was set according to their best SNR level in Fig. 2. As can be seen, 4D 4M maintained the LV myocardium uniformity very well, while the better results by ST121 methods were due to the (overly) smoothing effects both spatially and temporally. In Table 1 we also show the correlation coefficients (CC) between the reconstructed and Ideal TACs of an ROI on LV [14] by the different methods. There is a slight decrease in CC for 4D 4M compared to ST121 8M. One contributing factor to this decrease of CC (and the uniformity) may be the inclusion of

scatter compensation in 4D 4M, which adversely increases the image variance while increasing the contrast [14].

Table 1. Uniformity measure and correlation coefficient (CC) of time activity curves (TAC) of the LV wall reconstructed by different methods. (Standard deviations are in parentheses).

	Uniformity	CC of TAC
ST121 8M	9.52 (1.74)	0.6385 (0.2160)
ST121 4M	10.78 (2.07)	0.4168 (0.3201)
MAP-S 4M	20.39 (5.2)	0.3569 (0.2208)
4D 4M	11.77 (2.1)	0.5577 (0.2693)

Finally, in Fig. 5, we show a set of typical images reconstructed by the different methods from one noise realization. Again, for 3D 4M and 4D 4M the spatial parameter β_s was set according to their best SNR level in Fig. 2. For clarity, only one short-axis slice of the LV myocardium is shown for two different gates (end-diastole (ED) and end-systole (ES)). The noiseless reference images (Ideal) are also shown. The images from 4D 4M show significantly less noise artifacts and better definition of the LV wall.

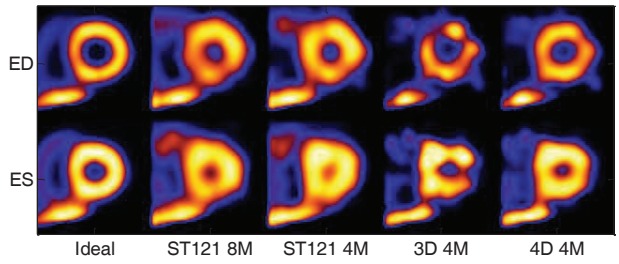


Fig. 5 Short-axis images reconstructed by different methods.

4. CONCLUSION

In this work, we investigated the utility of 4D reconstruction to lower the radiation dose of GSPECT. Our preliminary simulation results demonstrate that better or comparable performance, measured by various metrics on reconstruction accuracy and defect detectability, can be achieved by 4D reconstruction at half dose compared to clinical reconstruction at standard dose. These promising results warrant further comprehensive study for different compensation strategies as well as patient variability, which could pave the way for potential clinical studies. This could significantly improve the risk to benefit value of GSPECT for management of patients with cardiovascular disease.

5. REFERENCES

[1] Berrington de Gonzalez, A., K.P. Kim, *et al*., "Myocardial perfusion scans: projected population cancer risks from current levels of use in the United States," *Circulation.* 2010;122(23):2403-10.

[2] Williams, K. A. A historical perspective on measurement of ventricular function with scintigraphic techniques: part II - ventricular function with gated techniques for blood pool and perfusion imaging." *Journal of Nuclear Cardiology*. 12 (2005): 208-215.

[3] Mettler, F.A. Jr, B.R. Thomadsen BR, et al. Medical radiation exposure in the U.S. in 2006: preliminary results. *Health Phys*. 2008; 95:502–507.

[4] Eisenberg MJ, Afilalo J, Lawler PR, Abrahamowicz M, Richard H, Pilote L. Cancer risk related to low-dose ionizing radiation from cardiac imaging in patients after acute myocardial infarction. *CMAJ* 2011;183:430-6.

[5] DePuey G, Bommireddipalli S. Half-dose myocardial perfusion SPECT with wide beam reconstruction. *Circulation*. 2009;120: S334.

[6] Marcassa C, Campini R, Zoccarato O, Calza P. Wide beam reconstruction for half-dose or half-time cardiac gated SPECT acquisitions: optimization of resources and reduction in radiation exposure. *Eur J Nucl Med Mol Imaging.* 2011 Mar;38(3):499-508.

[7] He X, Links JM, Frey EC. An investigation of the trade-off between the count level and image quality in myocardial perfusion SPECT using simulated images: the effects of statistical noise and object variability on defect detectability. *Phys Med Biol.* 2010 Sep 7;55(17):4949-61.

[8] Lalush D S and Tsui B MW. Block-iterative techniques for fast 4D reconstruction using a priori motion models in gated cardiac SPECT. *Phys. Med. Biol*. 1998;43 875–86.

[9] Narayanan M V, King M, Wernick M N, Byrne C L, Soares E J and Pretorius P H. Improved image quality and computation reduction in 4D reconstruction of cardiac-gated SPECT images. *IEEE Trans. Med. Imaging*. 2000;19 423–33.

[10] Gilland D R, Mair B A, Bowsher J E and Jaszczak R J. Simultaneous reconstruction and motion estimation for gated cardiac ECT. *IEEE Trans. Nucl. Sci*. 2002; 49 2344–9.

[11] Brankov JG, Yang Y, Wernick MN. Spatiotemporal processing of gated cardiac SPECT images using deformable mesh modeling. *Med Phys*. 2005;32(9):2839-49.

[12] Gravier E, Yang Y, King MA and Jin M. Fully 4D motion-compensated reconstruction of cardiac SPECT images. *Phys. Med. Biol*. 2006;51:4603–19.

[13] Jin M, Yang Y, Niu X, Marin T, Brankov JG, Feng B, Pretorius PH, King MA, Wernick MN. A quantitative evaluation study of four-dimensional gated cardiac SPECT reconstruction. *Phys Med Biol.* 2009;54(18):5643-59.

[14] Niu, X., Y. Yang, M. Jin, M.N. Wernick, and M.A. King. Effects of motion, attenuation, and scatter corrections on gated cardiac SPECT reconstruction. *Med. Phys*., 2011; 38(12): 6571-84.

[15] Ljungberg M and Strand S V. A Monte Carlo program simulating scintillation camera imaging. *Comput. Methods Programs Biomed*. 1989;29:257–72.

[16] Segars W P. 2001. Development of a new dynamic NURBS-based cardiac-torso (NCAT) phantom. PhD Thesis, The University of North Carolina.

[17] Myers K J and Barett H H 1987 Addition of a channel mechanism to the ideal-observer model J. Opt. Soc. Am. A 4 2447–57.